RSC Advances

ROYAL SOCIETY OF CHEMISTRY

www.rsc.org/advances

N- and Fe-doped Carbon Nanotube/CMK3 Nanocomposite was firstly prepared by a simple procedure. The typical product shows excellent catalytic ability for oxygen reduction reaction in the acidic media.

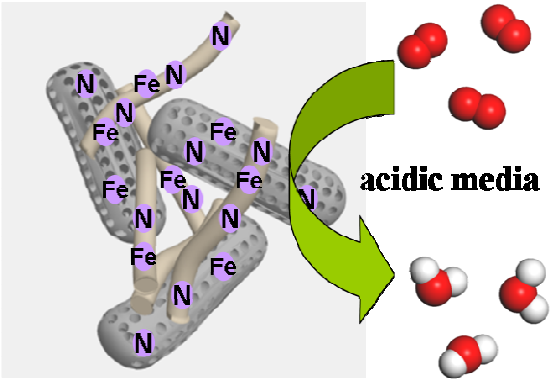

NFe-CNT/CMK-3

In Situ Formation of N- and Fe-doped Carbon Nanotube/ Mesoporous Carbon Nanocomposite with Excellent Activity for Oxygen Reduction in Acidic Media

Xiang-Jun Huang [a], Ya-Nan Luan [a], Peng-Fei Yao [a], Jin-Song Xie [b, *], Liang Yu [a], Zhen-Yu Wu [a], Ping Chen [a,*]

a School of Chemistry and Chemical Engineering, Anhui University, Hefei, Anhui, 230601, P. R. China

b Department of Chemistry and Materials Engineering, Hefei University, Hefei，Anhui, 230601,P.R.China

***Correspondence to:** Dr. P. Chen (E-mail: chenping@ahu.edu.cn); Dr. J. S. Xie (E-mail: xjs153@hfuu.edu.cn)

† Electronic supplementary information (ESI) available

Abstract

N- and Fe-doped Carbon Nanotube/CMK3 Nanocomposite (NFe-CNT/CMK3) was firstly prepared by a simple procedure. Trace Fe^{3+} can catalyze the *in situ* growth of the N- and Fe-doped Carbon Nanotube from the melamine as CNT precursor. The typical product shows excellent catalytic ability for oxygen reduction reaction (ORR) in the acidic media. The value of onset potential and half-peak potential of the typical product is only 68.0 mV and 63.0 mV less than that of the commercial 20 % Pt/C catalyst, respectively. The product also reveals superior stability and tolerance to methanol poisoning effects compared to the Pt/C. We believe that the NFe-CNT and NFe-CMK3

in the nanocomposite have the synergistically enhanced electrochemical activities for ORR in acidic media. The proposed method is simple and readily scalable. We anticipate such a nanoporous nanocomposite will have broad applications in the other fields such as supercapacitors, lithium ion batteries, gas uptake, biosensors, removal of pollutant and so on.

Introduction

In view of the increasingly serious energy crisis and the challenge of the greenhouse effect, fuel cell is one of the most promising to alternative energy sources because it has high power density and no any pollution.[1,2] Electrocatalysts for the oxygen reduction reaction (ORR) are crucial in fuel cells. Because of the scarcity of platinum, developing non-precious metal or metal-free electrocatalysts for ORR with high activity has been regarded as an important issue.[3-6] In the past several years, many high-performance ORR catalysts in the alkaline media have been developed.[7-12] However, it is well-known that proton exchange membrane (PEM) fuel cells can only be worked with acidic electrolytes. Unfortunately, the catalysts exhibit the dissatisfactory or even very weak ORR performance in acidic media.[6,13-15] The another important issue is, for the purpose of the practical application in the fuel cells, the ORR catalysts should be low-cost and high-volume production. Therefore, developing high-performance non-precious metal ORR electrocatalysts in acidic media with cheap and commercially available materials is a great challenge in the practical application of fuel cell.[5,16,17]

Recently, N-doped carbon materials have been a promising metal-free electrocatalysts for ORR, because of a large number of active sites and high conductivity.[18] Especially,

the N-doped carbon catalysts such as carbon nanotubes, graphene and carbon nanotube-graphene complexe have been developed and shown the ORR activity in acidic media.[19] The addition of certain transition metals to the nitrogen-doped carbon materials can improve the ORR activity in acidic media.[20,21] Fe and Co elements have been added to the carbon materials to improve the ORR activity because these metal cations can coordinate with the nitrogen doped in the carbon materials so as to increase the active sites for ORR.[22] However, in the design of these catalysts, careful selection of suitable nitrogen/transition-metal precursors and carbon supports is very important.[22-25]

Nitrogen-doped carbon nanotubes have received increasing attention as ORR catalysts, because of strong stability. In the past several years, some effective ORR catalysts based on the carbon nanotubes have been developed.[10,19,26]

In principle and fact, in order to improve the ORR activity, nanoscale porosity is highly desirable, which can facilitate high mass transfer fluxes.[27,28] It is well-known that the mesoporous carbon has the pore size ranging from 2 to 50 nm, so that it can be a potential candidate electrocatalyst because of the high surface area and various pore sizes [21,28-30] Very importantly, so far, great progress in the preparation of mesoporous carbon material has been made. For example, CMK-3 (an ordered mesoporous carbon) can be manufactured on the large scale at low-cost and has become the commercially available materials.[29,31]

Based on the above consideration and our recent study,[10,17,31-34] here, the N- and Fe-doped carbon nanotube/CMK3 nanocomposite (NFe-CNT/CMK3) was firstly prepared. We develop a facile and readily scalable approach to synthesize the low-cost

and excellent electrocatalyst for the ORR. The NFe-CNT and NFe-CMK3 in the nanocomposite have the synergistically enhanced electrochemical activities for ORR in acidic media.

Experimental methods

All reagents are of analytical reagent grade and used without further purification. CMK3 was purchased from Nanjing XFNANO Materials Tech Co., Ltd. The specific surface area, porosity and mean pore size of the CMK3 were provided in the Fig. S1.

Preparation of N- and Fe-doped Carbon Nanotube/CMK3 Nanocomposite (NFe-CNT/CMK3). Firstly, 60.0 mg CMK3 was dispersed in the 10 mL distilled water to form the mixture. Then, 6.0 mg $FeCl_3$ was added to the mixture, which was stirred magnetically at 25 ^oC for 50 min. The dried mixture was obtained by freeze drying for 12 h. Finally, the dried mixture and 500 mg melamine were mixed by grind process. Then the mixture was annealed in N_2 atmosphere at 950°C for 60 min and the final product was obtained. **Scheme1** shows the illustration of the *in situ* formation of typical NFe-CNT/CMK3 nanocomposite.

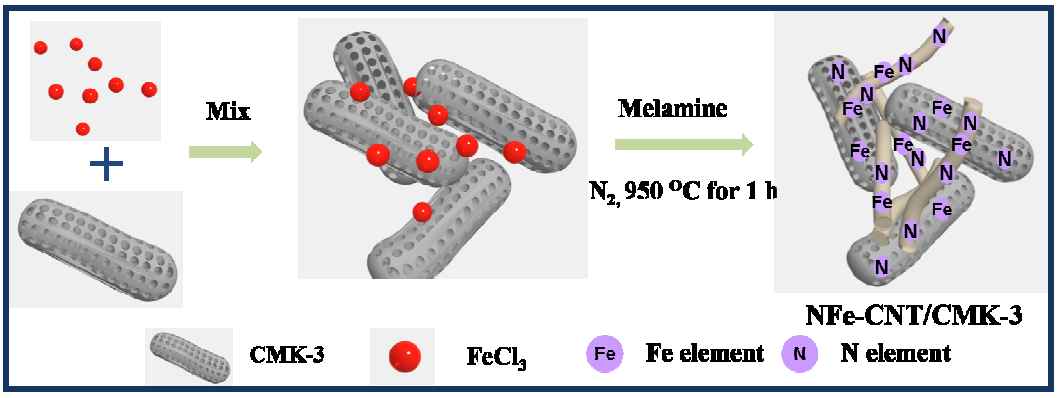

Scheme 1. Illustration of the preparation of the typical NFe-CNT/CMK3

Preparation of N- and Fe-doped Carbon Nanotube (NFe-CNT). NFe-CNT was made through the same steps as CMK3/CNT-N-Fe without adding CMK3 in the process.

Preparation of Fe-doped CMK3 (Fe-CMK3). Fe-CMK3 was made through the same steps as CMK3/CNT-N-Fe without adding melamine in the process.

Preparation of N-doped CMK3 (N-CMK3). N-CMK3 was made through the same steps as CMK3/CNT-N-Fe without adding $FeCl_3$ in the process.

Characterization. A JEM-2100F with an EDX analytical system was used to record the scanning transmission electron microscopy (STEM) images. STEM samples were prepared by drop-drying the products onto copper grids. Scanning electron microscopy (SEM) images were obtained on a field emission scanning electron microanalyzer (JEOL-6700F). SEM samples were prepared by drop-drying the samples onto silicon substrates. BET surface area was measured with a Micrometrics ASAP2020 analyzer (USA). X-ray photoelectron spectroscopic (XPS) results were obtained from an X-ray photoelectron spectrometer (ESCALab MKII). Raman spectra were taken by an inVia-Reflex spectrometer (Renishaw) with a 532 nm laser excitation.

Electrochemical measurements.

CHI 730E electrochemical workstation (Shanghai Chenhua, China) was used to test the electrocatalytical abilities for ORR. A platinum plate was used as counter electrode and Ag/AgCl was used as reference electrode. The ORR tests were carried out in O_2-saturated 0.5 M H_2SO_4 solution at room temperature. In the rotating disk electrode

(RDE) measurements, the working electrode is a glassy carbon (GC) disk with a diameter of 5 mm. For each sample (including the commercial 20 % Pt/C), 10.0 mg of the sample was dispersed in the ethanol solution (5.0 mL) and ultrasonically for 40 min. Then, 12.0 μL of this suspension was dropped and adhered on the GC disk electrode using Nafion solution.[10,17] In the rotating ring-disk electrode (RRDE) measurements, catalyst and electrode were prepared by the same method as RDE. Pt ring electrode was polarized at 850 mV (vs / RHE) in O_2-saturated 0.5 M H_2SO_4.

The calibration of Ag/AgCl electrode was performed in a standard three-electrode system with polished Pt wires as the working and counter electrodes, and the Ag/AgCl electrode as the reference electrode. Electrolytes are pre-purged and saturated with high purity H_2. In 0.5 M H_2SO_4, E (RHE) = E (Ag/AgCl) + 0.23 V.[17]

Results and discussion

The representative SEM and TEM images of the typical NFe-CNT/CMK3 were shown in the Fig. 1a and Fig. S2 (see Supporting Information). These results clearly revealed the typical NFe-CNT/CMK3 contains CMK3 and carbon nanotubes with the diameter from 100 to 230 nm. STEM image of the typical NFe-CNT/CMK3 were shown in the Fig. 1b. From the element mapping (Fig. 1c-f), the product contains carbon, oxygen, nitrogen and ferrum elements. Fig. S3a and b (see Supporting Information) shows the elemental analysis data in the square region marked with 1 and 2 in the Fig. 1b, respectively. The product in the square region marked with 1 and 2 was doped by the nitrogen and ferrum elements, respectively. However, the square region marked with 2

contains higher nitrogen and ferrum content than that marked with 1. The SEM images also indicate that the CMK3 and carbon nanotubes can produce a three-dimension interpenetrated network structure.

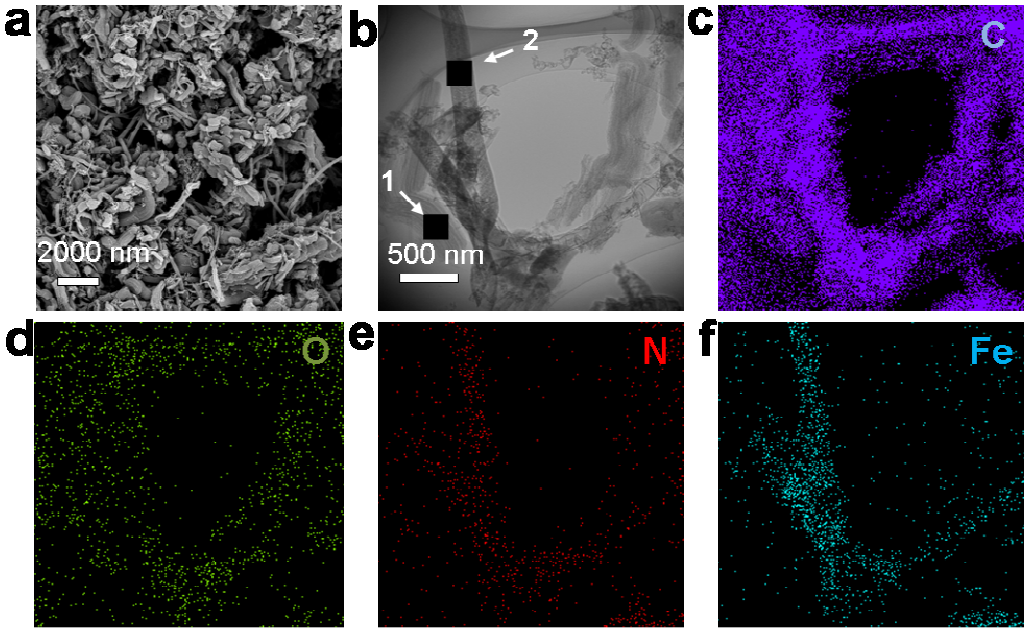

Fig. 1. (a-b) SEM and STEM images of the typical NFe-CNT/CMK3; (c-f) carbon, oxygen, nitrogen, ferrum and element mapping.

XPS full-scale spectrum of the typical NFe-CNT/CMK3 and the high-resolution N1s XPS spectrum were shown in the Fig. 2a-b. From the Fig. 2a, the product contains carbon, oxygen, nitrogen and ferrum elements. Fig. 2b indicates three kinds of nitrogen were doped. The peak at 398.1 eV can be ascribed to pyridinic N species, the peak at 400.2 eV can be ascribed to pyrrolic structure and the peak at 401.2 eV corresponds to the graphitic N.[10,17] According to the XPS data, 2.73 at.% of the N and 0.30 at.% of the Fe were doped in the typical product. Fig. 2c shows the N_2 adsorption–desorption isotherms. The BET surface area, total pore volume and micropore volume of the

typical product was 862.00 $m^2 g^{-1}$, 0.53 $cm^3 g^{-1}$ and 0.33 $cm^3 g^{-1}$, respectively. Raman spectra (Fig. 2d) show that the typical product exhibits the remarkable peaks at around 1335 and 1588 cm^{-1} corresponding to the D band and G band, respectively. In addition, a broader 2D peak appeared at around 2850 cm^{-1}.

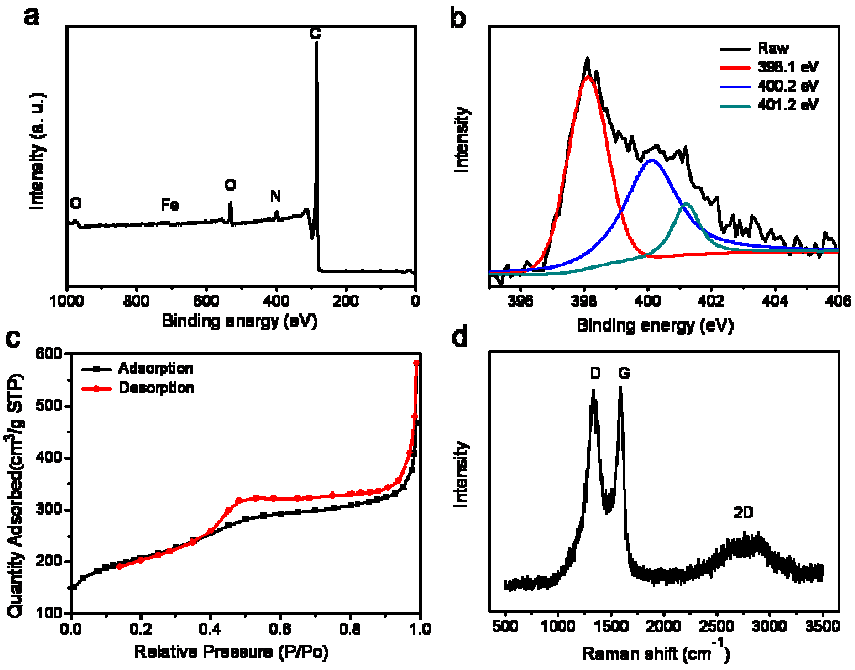

Fig. 2. (a) XPS full-scale spectrum; (b) high-resolution N1s XPS spectrum; (c) adsorption-desorption isotherm and (d) Raman spectra of the typical NFe-CNT/CMK3.

We also prepared the N-CMK3, Fe-CMK3 and NFe-CNT. SEM images of these samples were shown in the Fig. 3. From the Fig. 3a, the NFe-CNT mainly contains carbon nanotubes with the diameter from 30 to 50 nm. From the Fig. 3b and c, N-CMK3 and Fe-CMK3 contain the mesoporous carbon without carbon nanotubes, respectively. Fig. S4 (see Supporting Information) shows the XPS full-scale spectra of the N-CMK3, Fe-CMK3 and NFe-CNT samples. From the Fig. S4, the N-CMK3 was doped by nitrogen, Fe-CMK3 was doped by ferrum and NFe-CNT was doped by

nitrogen and ferrum elements. In addition, we also prepared the product by simply mixing the raw reagents of melamine, CMK3, and $FeCl_3$, without the subsequen t pyrolysis. The product was denoted as mixture product. The XPS full-scale spectrum and high-resolution N1s XPS spectrum were shown in the Fig. S5a and b (see Supporting Information). According to the XPS data, the mixture product contains the 60.61 at.% of the C, 34.71 at.% of the N, 4.14 at.% of the O,and 0.54 at.% of the Fe. The N1s XPS peak of the mixture product comes from the raw materials of melamine.

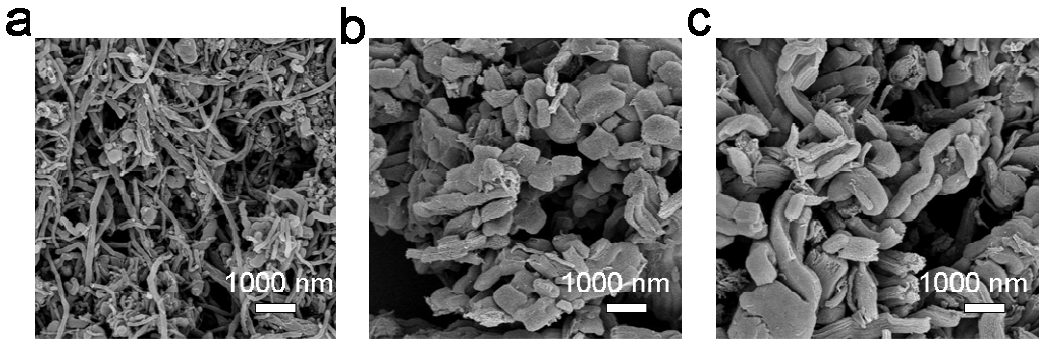

Fig. 3. SEM images of the NFe-CNT (a), N-CMK3 (b) and Fe-CMK3 (c)

We also prepared the products when the different $FeCl_3$ (3, 4, 10 and 15 mg) were added in the preparation. These products were denoted with NFe-CNT/CMK3-3mg, NFe-CNT/CMK3-4mg, NFe-CNT/CMK3-10mg and NFe-CNT/CMK3-15mg. Fig. 4 shows the SEM images of the samples. From the Fig. 1 and 4, controlling the appropriate ratio of $FeCl_3$ to CMK3 content is crucial in the produce of the carbon nanotube. When the ratio of $FeCl_3$ to CMK3 (w/w) is 1/10, the typical product has more carbon nanotubes than others.

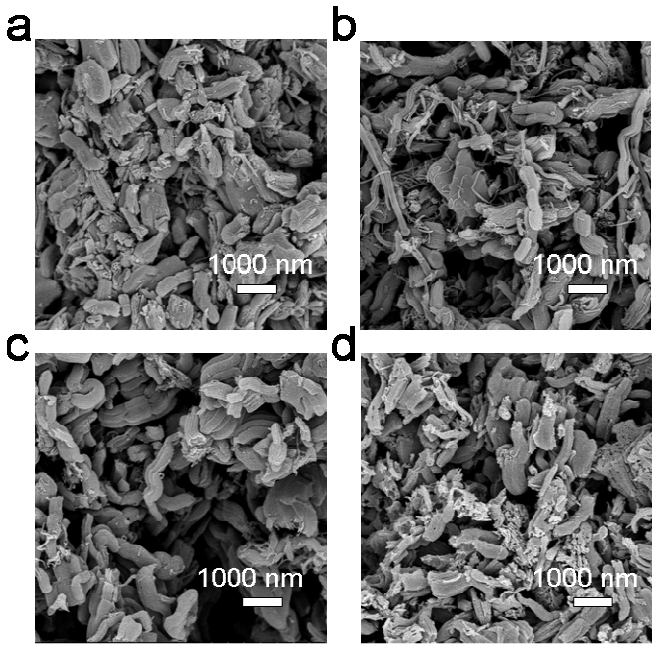

Fig. 4. SEM images of the NFe-CNT/CMK3-3mg (a), NFe-CNT/CMK3-4mg (b), NFe-CNT/CMK3-10mg (c) and NFe-CNT/CMK3-15mg (d)

Electrocatalytic activities

We tested the ORR activities of the samples in the acidic media (0.5 M H_2SO_4). ORR activities were measured by rotating disk electrode (RDE) and rotating ring-disk electrode (RRDE) technologies.[17] For comparison, commercial platinum (20 wt %) on carbon black (Pt/C) (Johnson Matthey) was also tested. Fig. 5 shows the ORR results. From the Fig. 5a, for the typical product and Pt/C, the value of onset potential was 803.0 and 871.0 mV (vs RHE), respectively. Obviously, the value of onset potential and half-peak potential of the typical product is only 68.0 mV and 63.0 mV less than that of the Pt/C, respectively. When the potential is lower than 670.0 mV (vs RHE), the current density of the typical product electrode is remarkably larger than that of commercial Pt/C.

For the NFe-CNT, N-CMK3 and Fe-CMK3, the value of onset potential was 730, 670,

and 685 mV (vs RHE), respectively. For the NFe-CNT/CMK3, N-CMK3, Fe-CMK3 and NFe-CNT, the typical NFe-CNT/CMK3 shows the highest value of onset and half-peak potential and largest reduce current. So far, though many ORR catalysts have shown the excellent activity and durability in alkaline solution, it remains a great challenge to achieve the excellent ORR activity and durability in acidic media. According to the reported literature, the typical product exhibits the very high ORR activity and excellent durability in acidic media.[2,5,13,14,16,19,21,24,35] RDE voltammograms for the ORR on the typical product at the various rotation speeds (from 400 to 2000 rpm) was shown in the Fig. 5b. RDE voltammograms on the Pt/C, N-CMK3, Fe-CMK3 and NFe-CNT at the various rotation speeds (from 400 to 2000 rpm) was shown in the Fig. 6a-d. From the Fig. 5b and Fig. 6a, the half-peak potential of the typical product is only 59, 61, 62, 63.0 and 65 mV less than that of the Pt/C at the rotation speeds from 400 to 2000 rpm, respectively. From the Fig. 5b and Fig. 6b-d, the typical NFe-CNT/CMK3 also shows the higher value of onset and half-peak potential and larger reduce current at the rotation speeds from 400 to 2000 rpm than the N-CMK3, Fe-CMK3 and NFe-CNT, respectively.

An ideal ORR catalyst should have satisfactory tolerance to the fuel molecules. In this work, methanol poisoning effects of the typical product and commercial Pt/C were investigated. We measured the poisoning effects of the typical NFe-CNT/CMK3 in O_2-saturated 0.5 M H_2SO_4 with 0.5, 1.5 and 3.0 M methanol, respectively. The results were shown in the Fig. 5c. We also measured the poisoning effects of the Pt/C in O_2-saturated 0.5 M H_2SO_4 with 1.0 M methanol (shown in the Fig. S6, see Supporting

Information). Compared to Pt/C, the typical product shows little activity loss, which indicates that the typical product has excellent tolerance to methanol poisoning effects. The typical NFe-CNT/CMK3 still has excellent tolerance to the methanol in O_2-saturated 0.5 M H_2SO_4 with 3.0 M methanol. Durability of the typical NFe-CNT/CMK3 and Pt/C was measured by the current-time (i-t) chronoamperometric response. The results were shown in the Fig. 5d. After 10000 seconds, the Pt/C suffered from a 22.5 % loss in current density while the typical product showed the 18.8 % decrease of current density, which indicates the NFe-CNT/CMK3 has a better durability than the Pt/C.

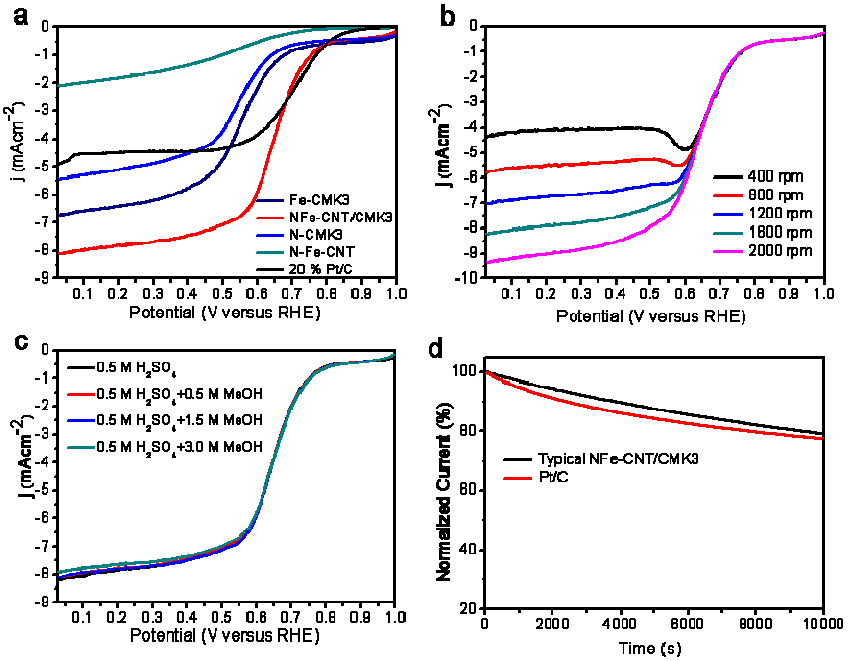

Fig. 5. RDE results in 0.5 M H_2SO_4. (a) RDE voltammograms in O_2-saturated 0.5 M H_2SO_4 at room temperature (rotation speed 1600 rpm, sweep rate 20 mV s^{-1}) for the typical NFe-CNT/CMK3, N-CMK3, Fe-CMK3, NFe-CNT and Pt/C; (b) RDE voltammograms for the ORR at the typical NFe-CNT/CMK3 electrode at the various rotation speeds (sweep rate 20 mV s^{-1}); (c) RDE voltammograms in O_2-saturated 0.5 M H_2SO_4 at room temperature (rotation speed 1600 rpm, sweep rate 20 mV s^{-1}) for the typical NFe-CNT/CMK3 with or without methanol; (d) Current-time (i-t) chronoamperometric response of the typical NFe-CNT/CMK3 and Pt/C electrodes at

-0.65 V (vs Hg/HgO) in O_2-saturated 0.5 M H_2SO_4 at a rotation rate of 700 rpm.

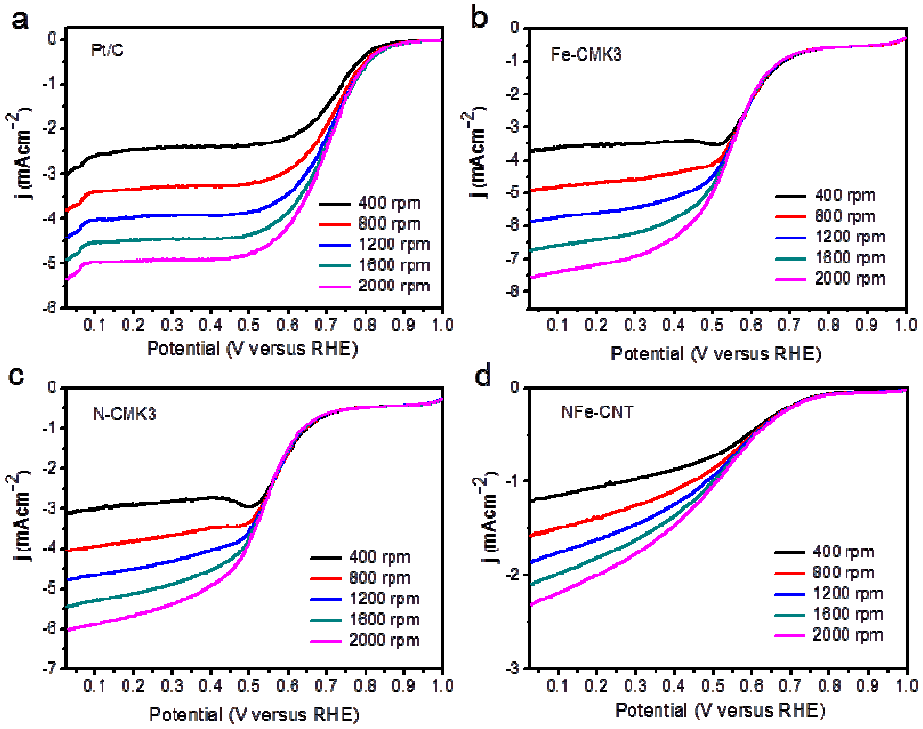

Fig. 6. (a-d) RDE voltammograms for the ORR at the Pt/C，Fe-CMK3, N-CMK3 and NFe-CNT electrode at the various rotation speeds (sweep rate 20 mV s^{-1})

Effect of the Fe content, annealing temperature and time on the ORR activity were investigated. The results were shown in the Fig.7. Fig.7a shows the effect of Fe content on the ORR activity. From the Fig. 7a, the optimal $FeCl_3$ amount is 6 mg in the typical preparation. We also prepared the products when the temperature is 850 ^oC, 950 ^oC and 1000 ^oC in the preparation, respectively. These products were denoted with NFe-CNT/CMK3-850, NFe-CNT/CMK3-950 and NFe-CNT/CMK3-1000. Fig. 7b shows the effect of annealing temperature on the ORR activity. Fig. 7c shows the effect of annealing time (when the temperature is 950 ^oC) on the ORR activity. From the Fig.

7b-c, the optimal annealing temperature and time is 950 ^{o}C and 60 min. From the Fig. 7, we can easily draw a conclusion that Fe content, annealing temperature and annealing time can obviously affect the ORR activity.

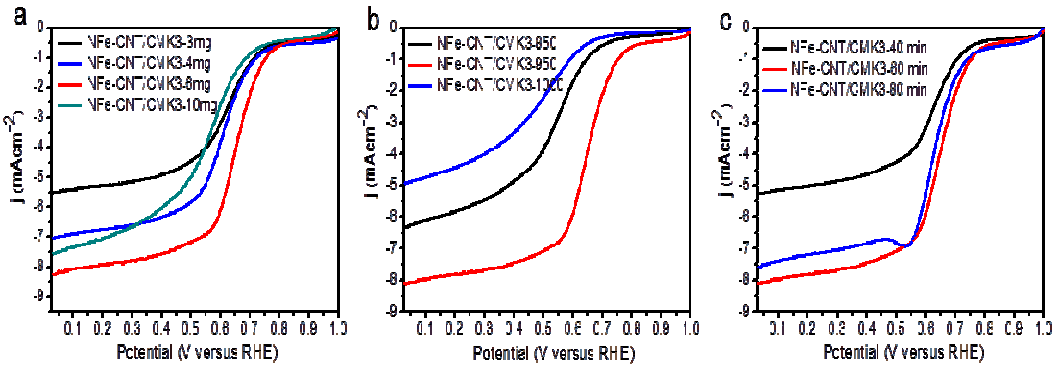

Fig. 7. (a) RDE voltammograms in O_2-saturated 0.5 M H_2SO_4 at room temperature (rotation speed 1600 rpm, sweep rate 20 mV s^{-1}) for the NFe-CNT/CMK3-3mg, NFe-CNT/CMK3-4mg, NFe-CNT/CMK3-6mg and NFe-CNT/CMK3-10mg; (b) RDE voltammograms in O_2-saturated 0.5 M H_2SO_4 at rotation speed 1600 rpm, for the NFe-CNT/CMK3-850, NFe-CNT/CMK3-950 and NFe-CNT/CMK3-1000; (c) RDE voltammograms in O_2-saturated 0.5 M H_2SO_4 at rotation speed 1600 rpm, for the NFe-CNT/CMK3-40min, NFe-CNT/CMK3-60min and NFe-CNT/CMK3-80min

The selectivity of the four-electron reduction of oxygen on the typical NFe-CNT/CMK3 and Pt/C was investigated by the RRDE technology. The four-electron selectivity was evaluated based on the H_2O_2 yield. The H_2O_2 yield and the electron transfer number (n) were determined by the following equations:

$$\%(H_2O_2) = 200 \times \frac{I_R / N}{I_D + I_R / N} \qquad (1)$$

$$n = 4 \times \frac{I_D}{I_D + I_R / N} \qquad (2)$$

where I_D is the disk current, and I_R is the ring current, and N is current collection efficiency of the Pt ring.[7,17] N is 0.35 from the reduction of $K_3Fe[CN]_6$.

Fig. 8 shows the RRDE voltammograms for the typical NFe-CNT/CMK3, from which

the peroxide yield and electron transfer number were obtained (Fig. 8b). The peroxide yield remained below 0.5 % at the potentials from 0.05-1.0 V (versus RHE) and electron transfer number was calculated to be 3.90-4.00, which reveals an intrinsic four-electron-transfer process. For the Pt/C (Fig. 8c and d), the peroxide yield remained below 4.0 % at the potentials from 0.05-1.0 V (versus RHE) and electron transfer number was calculated to be 3.95-4.00.

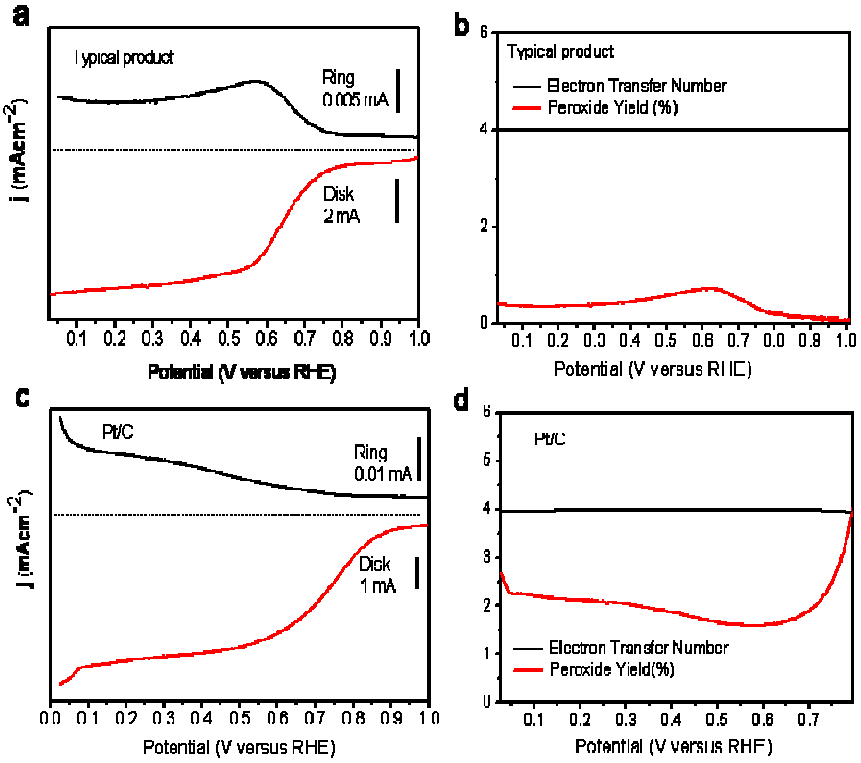

Fig. 8. RRDE results for the typical NFe-CNT/CMK3 and Pt/C**.** (a) RRDE voltammograms for the ORR at the typical NFe-CNT/CMK3 electrode in O_2-saturated 0.5 M H_2SO_4. The electrode rotation speed was 1600 rpm, sweep rate was 20 mV s^{-1}; (b) The electron transfer number (n) and peroxide yield obtained from RRDE curve Fig. 8a; (c) RRDE voltammograms for the ORR at the Pt/C electrode in O_2-saturated 0.5 M H_2SO_4; (d) The electron transfer number (n) and peroxide yield obtained from RRDE curve Fig. 8c.

What is the reason for the excellent ORR activity of the NFe-CNT/CMK3 in acidic

media? We believe that the NFe-CNT and NFe-CMK3 in the nanocomposite have the synergistically enhanced electrochemical activities for ORR in acidic media. The doping of the nitrogen and ferrum elements in the NFe-CNT/CMK3 can promote the activity of ORR catalysts in acidic media, because the ferrum element can coordinate with the nitrogen doped in the carbon materials so that the more active site can be produced.[20,23,24] Combining the NFe-CMK3 with the NFe-CNT can form a three-dimension interpenetrated network structure, which can improve conductivity of the nanocomposite and highly effectively accelerates reactant, ion and electron transport.[10,17] In addition, the nanocomposite has large surface area so that it has many catalytic sites for ORR on the surface, and the active sites can be easily exposed to react.[21,28,36,37]

Nowadays, CMK-3 can be manufactured on the large scale at low-cost and has become the commercially available materials. The NFe-CNT/CMK3 nanocomposite can be prepared by the simple and readily scalable procedure proposed by us. Therefore, this work is of great importance in the developing of high-performance non-precious metal electrocatalysts with cheap and commercially available materials. Because the obtained products have excellent catalytical ability in acidic media, they may have the practical application of fuel cell.[16,28,38,39] In addition, because of the doping of nitrogen and ferrum elements, three-dimension interpenetrated network structure and large surface area, the nanocomposite may have the broad applications in the other fields such as removal of pollutant, gas uptake, supercapacitors, lithium ion batteries, sensors and so on.

Conclusions

We developed a simple and readily scalable procedure to prepare the NFe-CNT/CMK3 nanocomposite. Trace Fe^{3+} can catalyze the *in situ* growth of the N- and Fe-doped CNT from the melamine as the precursor. The typical product shows excellent catalytic ability for oxygen reduction reaction (ORR) in the acidic media. The value of onset potential and half-peak potential of the typical product is only 68.0 mV and 63.0 mV less than that of the commercial 20 % Pt/C catalyst, respectively. The product also reveals superior stability and tolerance to methanol poisoning effects compared to the Pt/C. As an ordered mesoporous carbon, CMK-3 can be manufactured on the large scale at low-cost and has become the commercially available materials. This work is of great importance in the developing of high-performance non-precious metal electrocatalysts with cheap and commercially available materials. Because the obtained products have excellent catalytical ability in acidic media, they may have the practical application of fuel cell.

Acknowledgements

We acknowledge the funding support from the National Natural Science Foundation of China (Grants 21271005), Project of Anhui University (02303203-0054), the College Students' Innovation and Entrepreneurship Training Project (J18515020)，the Natural Science Foundation of Anhui Province (No.1308085QB35) and the Natural Science Foundation of Education Department of Anhui Province (No. KJ2015A232).

References

1. B. C. H. Steele and A. Heinzel, *Nature*, 2001, **414**, 345-352.
2. Y. H. Bing, H. S. Liu, L. Zhang, D. Ghosh and J. J. Zhang, *Chem. Soc. Rev.,* 2010, **39**, 2184-2202.
3. R. Bashyam and P. Zelenay, *Nature,* 2006, **443**, 63-66.
4. R. B. Levy and M. Boudart, *Science,* 1973, **181,** 547-549.
5. M. K. Debe, *Nature,* 2012, **486**, 43-51.
6. F. Jaouen, E. Proietti, M. Lefevre, R. Chenitz, J. P. Dodelet, G. Wu, H. T. Chung, C. M. Johnston and P. Zelenay, *Energ. Environ. Sci*., 2011, **4,** 114-130.
7. Y. Y. Liang, Y. G. Li, H. L. Wang, J. G. Zhou, J. Wang, T. Regier and H. J. Dai, *Nat. Mater.,* 2011, **10**, 780-786.
8. H. T. Chung, J. H. Won and P. Zelenay, *Nat. Commun.,* 2013, **4**,
9. P. Chen, T. Y. Xiao, H. H. Li, J. J. Yang, Z. Wang, H. B. Yao and S. H. Yu, *Acs Nano,* 2012, **6**, 712-719.
10. P. Chen, T. Y. Xiao, Y. H. Qian, S. S. Li and S. H. Yu, *Adv. Mater.*, 2013, **25**, 3192-3196.
11. S. J. Guo, S. Zhang, L. H. Wu and S. H. Sun, *Angew. Chem. Int. Edit.,* 2012, **51**, 11770-11773.
12. Y. Y. Liang, H. L. Wang, J. G. Zhou, Y. G. Li, J. Wang, T. Regier and H. J. Dai, *J. Am. Chem. Soc.* , 2012, **134**, 3517-3523.
13. C. Medard, M. Lefevre, J. P. Dodelet, F. Jaouen and G. Lindbergh, *Electrochim. Acta.,* 2006, **51**, 3202-3213.
14. J. Tian, L. Birry, F. Jaouen and J. P. Dodelet, *Electrochim. Acta.*, 2011, **56**, 3276-3285.
15. F. Charreteur, F. Jaouen, S. Ruggeri and J. P. Dodelet, *Electrochim. Acta*., 2008, **53**, 2925-2938.
16. G. Wu and P. Zelenay, *Acc. Chem. Res.,* 2013, **46**, 1878-1889.
17. P. Chen, L. K. Wang, G. Wang, M. R. Gao, J. Ge, W. J. Yuan, Y. H. Shen, A. J. Xie and S. H. Yu, *Energ. Environ. Sci.,* 2014, **7**, 4095-4103.
18. Y. Zheng, Y. Jiao, M. Jaroniec, Y. G. Jin and S. Z. Qiao, *Small,* 2012, **8**, 3550-3566.
19. Y. G. Li, W. Zhou, H. L. Wang, L. M. Xie, Y. Y. Liang, F. Wei, J. C. Idrobo, S. J. Pennycook and H. J. Dai, *Nat. Nanotechnol.,* 2012, **7**, 394-400.
20. M. Lefevre, E. Proietti, F. Jaouen and J. P. Dodelet, *Science,* 2009, **324**, 71-74.
21. H. W. Liang, W. Wei, Z. S. Wu, X. L. Feng and K. Mullen, *J. Am. Chem. Soc.,* 2013, **135**, 16002-16005.
22. G. Wu, K. L. More, C. M. Johnston and P. Zelenay, *Science,* 2011, **332**, 443-447.
23. U. I. Kramm, J. Herranz, N. Larouche, T. M. Arruda, M. Lefevre, F. Jaouen, P. Bogdanoff, S. Fiechter, I. Abs-Wurmbach, S. Mukerjee and J. P. Dodelet, *Phys. Chem. Chem. Phys.,* 2012, **14**, 11673-11688.
24. H. L. Peng, Z. Y. Mo, S. J. Liao, H. G. Liang, L. J. Yang, F. Luo, H. Y. Song, L. Zhong and B. Q. Zhang, *Sci. Rep-Uk,* 2013, **3**,
25. F. Jaouen, F. Charreteur and J. P. Dodelet, *J. Electrochem. Soc.,* 2006, **153**, A689-A698.
26. K. P. Gong, F. Du, Z. H. Xia, M. Durstock and L. M. Dai, *Science,* 2009, **323**, 760-764.
27. J. Y. Cheon, T. Kim, Y. Choi, H. Y. Jeong, M. G. Kim, Y. J. Sa, J. Kim, Z. Lee, T. H. Yang, K. Kwon, O. Terasaki, G. G. Park, R. R. Adzic and S. H. Joo, *Sci. Rep-Uk,* 2013, **3**,
28. J. Wang, H. L. Xin and D. L. Wang, *Part. Part. Syst. Char.,* 2014, **31**, 515–539.
29. S. Jun, S. H. Joo, R. Ryoo, M. Kruk, M. Jaroniec, Z. Liu, T. Ohsuna and O. Terasaki, *J. Am. Chem. Soc.,* 2000, **122**, 10712-10713.

30. J. Tang, T. Wang, X. Sun, Y. Y. Hu, Q. Q. Xie, Y. X. Guo, H. R. Xue and J. P. He, *Electrochim. Acta.,* 2013, **90**, 53-62.

31. X. J. Huang, Y. G. Tang, L. F. Yang, P. Chen, Q. S. Wu and Z. Pan, *J. Mater. Chem. A,* 2015, **3**, 2978-2984.

32. Z. Y. Wu, P. Chen, Q. S. Wu, L. F. Yang, Z. Pan and Q. Wang, *Nano Energy,* 2014, **8**, 118-125.

33. W. J. Yuan, J. C. Li, A. J. Xie, P. Chen, S. K. Li and Y. H. Shen, *Electrochim. Acta.,* 2015, **165**, 29-35.

34. W. J. Yuan, J. C. Li, L. K. Wang, P. Chen, A. J. Xie and Y. H. Shen, *Acs. Appl. Mater. Inter.,* 2014, **6**, 21978-21985.

35. C. Z. Zhu and S. J. Dong, *Nanoscale,* 2013, **5**, 1753-1767.

36. L. M. Dai, D. W. Chang, J. B. Baek and W. Lu, *Small,* 2012, **8**, 1130-1166.

37. H. Wang, X. J. Bo, Y. F. Zhang and L. P. Guo, *Electrochim. Acta.*, 2013, **108**, 404-411.

38. J. Tian, A. Morozan, M. T. Sougrati, M. Lefevre, R. Chenitz, J. P. Dodelet, D. Jones and F. Jaouen, *Angew. Chem. Int. Edit.,* 2013, **52**, 6867-6870.

39. J. Liu, X. J. Sun, P. Song, Y. W. Zhang, W. Xing and W. L. Xu, *Adv. Mater.,* 2013, **25**, 6879-6883.